

Project Number 282910

ÉCLAIRE

Effects of Climate Change on Air Pollution Impacts and Response Strategies for European Ecosystems

Seventh Framework Programme

Theme: Environment

D7.5 Source-receptor matrices of Air Pollution Metrics for current and future conditions

Due date of deliverable: **31/10/2014**

Actual submission date: **30/09/2015**

Start Date of Project: **01/10/2011**

Duration: **48 months**

Organisation name of lead contractor for this deliverable :

Norwegian Meteorological Institute

Project co-funded by the European Commission within the Seventh Framework Programme		
Dissemination Level		
PU	Public	
PP	Restricted to other programme participants (including the Commission Services)	X
RE	Restricted to a group specified by the consortium (including the Commission Services)	
CO	Confidential, only for members of the consortium (including the Commission Services)	

Source-receptor matrices of Air Pollution Metrics for current and future conditions

Executive Summary

A typical and arguably most important use of the EMEP model is to provide 'source-receptor' (SR) matrices, in which the model calculates the effects of reducing emissions in one country, and calculates the resulting impact on air pollution metrics in other countries, or in fact over all grid-cells of Europe. In this work the EMEP model has been used to conduct such SR calculations for current (year 2010) and future (2050) scenarios.

In the ECLAIRE project, and as reported in Deliverable D7.2, the EMEP model has been enhanced so that it can take account of a number of changes which are expected in a future climate. In this report we examine how calculated SR results change when these climate enhancements are taken into account, and also compare with changes due to simple emission scenarios.

The main conclusion from these runs is that in most cases the impacts of climate-change itself (e.g. CO₂ inhibition of isoprene emissions or stomatal conductance) do not change the basic SR estimates very much, and that the main driver of changes is rather the difference in emissions between the 2010 and 2050 cases. The main exception was for phyto-toxic ozone dose to crops (POD₃-IAM-CR), where the assumptions concerning climate response of stomatal conductance had an appreciable impact on the base-levels of POD₃ and on the responses to NO_x emission reduction.

1 Objectives

The objectives of D7.5 are to assess how changing climate will impact the calculation of source-receptor matrices over Europe.

2 Activities

The EMEP MSC-W model is a well verified chemical transport model, designed for the prediction of pollutants such as ozone and acidifying and eutrophying compounds, and particulate matter (Simpson et al. 2006, 2012, Fagerli and Aas 2008). A typical and arguably most important use of the EMEP model is to provide 'source-receptor' (SR) matrices, in which the model calculates the effects of reducing emissions in a source region (usually a country) on air pollution in receptor regions. In fact, as the EMEP model is always run for the full European domain in such calculations, the receptor can be thought of as any or all model grid-cells, or also in terms of countries.

In the ECLAIRE project, and as reported in Deliverable D7.2, the EMEP model has been enhanced so that it can take account of a number of changes which are expected in a future climate. In this report we examine how calculated SR results when these climate enhancements are taken into account, and also compare with changes due to simple emission scenarios.

2.1 Climate enhancements

The climate enhancements to the EMEP model used in this report can be summarised:

1. Increased NH₃ emissions in a warmer climate
2. CO₂ inhibition of isoprene emissions
3. CO₂ inhibition of stomatal conductance

Further discussion of these changes and their background and uncertainty can be found in Deliverable D7.2, but we summarise here the practical changes in terms of model implementation. Further ECLAIRE work on climate impacts (including the impacts of meteorological driver, growing seasons and even insect-induced stresses) can be found in related papers Bergström et al. (2014), Langner et al. (2012a,b), Sakalli and Simpson (2012), Simpson et al. (2014b), with further discussion of the uncertainties surrounding climate-effects in Simpson et al. (2014a).

2.1.1 Increased NH₃ emissions

Three papers arising from the ECLAIRE project have drawn attention to the possibility of quite significant increases in NH₃ emissions in the future as a result of increasing evaporation from sources such as animal manure (Sutton et al. 2013, Skjøth and Geels 2013), and the potentially important detrimental effect on N-deposition and critical load exceedances (Simpson et al. 2014b).

The projected increase will of course depend heavily on the projected temperature change and hence on the applied climate model, as well as assumptions concerning NH₃ emission factors. However, based on the above studies, Simpson et al. (2014b) explored the potential impact of a 20 and 30 % increase in NH₃ emissions for the future (2050s) scenarios.

In this work, we assume a climate-induced NH₃ emission increase of 20%, and refer to this as the A20 (or A20-NH₃) scenario.

2.1.2 Isoprene - CO₂ inhibition

It has been shown that increasing CO₂ can inhibit isoprene metabolism, and some studies suggest that higher CO₂ levels will reduce BVOC emission rates (e.g. Arneth et al. 2007, Wilkinson et al. 2009, Possell et al. 2005, Possell and Hewit 2011). The overall effect of increased CO₂ on BVOC emission rates is still unclear, even with regard to the sign of such changes (see also discussions in Simpson et al. (2014a)).

For this work, we have implemented the isoprene-CO₂ inhibition function of Wilkinson et al. (2009) into the EMEP model. For a CO₂ concentration of ca. 500 ppm (ca. 2050 levels consistent with the 2050 scenarios used in ECLAIRE), this produces a reduction in emission rates of 9%.

2.1.3 Stomatal sensitivity

D7.2 explored two methodologies for the CO₂-effect on stomatal conductance (g_{sto}). For the source-receptor tests we make use of the so-called K2011 method, based upon Klingberg et al. (2011), since this methodology is fully consistent with standard EMEP model g_{sto} calculations used in the S-R calculations for current years. Klingberg et al. (2011) modelled the effect of CO₂ on g_{sto} with a much simpler algorithm. The influence of increasing CO₂ on g_{sto} was assumed to linearly decrease between 360 and 560 ppm CO₂ concentration from 1 to 0.66 for a generic crop and to 0.8 for a generic deciduous tree, with no further reductions in g_s above 560 ppm CO₂.

2.2 Approach

We have first calculated a number of base-cases, against which SR calculations can be compared:

Base-case	Label	Description
(a) 2010-Base		Emissions of 2010, standard model setup
(b) 2050-Base		Emissions of 2050, standard model setup
(c) 2050-A20	A20-NH ₃	as (b), plus 20% more NH ₃ emission
(c) 2050-BVOC	CO ₂ -BVOC	as (b), with CO ₂ inhibition of isoprene emissions
(d) 2050-KCO2	CO ₂ - g_{sto}	as (b), with CO ₂ inhibition of stomatal conductance

For each of these cases, we have calculated the impact of either a 15% reduction in NO_x or a 15% reduction in NH₃. We present example calculations for four countries, selected to cover different geographical and pollution climates in Europe: Netherlands (NL), Poland (PL), Spain (ES) and Italy (IT). (Full source-receptor matrices for all countries for recent years can be found at www.emep.int.)

The EMEP model produces many outputs, but to keep this report manageable we focus on four important metrics (Table 1).

Table 1: Air Pollution Metrics used in this report; abbreviations and units

Metric	units	
TDEP-OXN	mg(N) m ⁻² yr ⁻¹	Total deposition of oxidised nitrogen, important for acidification, eutrophication and generally an indicator of nitrogen oxides in the environment
TDEP-RDN	mg(N) m ⁻² yr ⁻¹	Total deposition of reduced nitrogen, important for acidification, eutrophication and important since many scenarios predict an increase in NH ₃ emissions.
SOMO35	ppb.days	Annual sums of daily maximum running 8 h average O ₃ concentrations above 35 ppb, a metric recommended for health impacts by WHO (Amann et al. 2008).
POD3-IAM-CR	mmole O ₃ m ⁻² yr ⁻¹	Phyto-toxic ozone dose with threshold 3 nmole m ⁻² s ⁻¹ . This metric is an indicator of risks to vegetation, see LRTAP (2009), Mills et al. (2011).

3 Results

3.1 NOy deposition

Tables 2-5 present the results of the different SR calculations for total NOy deposition (TDEP-OXN). Results are here presented as domain-averages, for the five base-cases (one for 2010, four for 2050), and the impact of 15% reductions in emissions of NOy and NH₃. As expected, the reductions in NOy emissions have a far larger effect than reductions in NH₃ emissions. The other main feature of the results from all countries is that the impact of the NOy or NH₃ is much smaller than the impact of the same (relative) changes in 2010. In fact, the different climate scenarios are essentially identical, so that the SR results from the more complex scenarios (e.g. KCO2) cannot be distinguished from those of the simple 2050-Base results.

Figures 1-4 illustrate these SR calculations in more detail. For example, Fig. 1(a) shows the straightforward change, Δ TDEP-OXN, in oxidised nitrogen deposition between the base-case run for 2050 and a run with 15% reduced emissions of NOx. This reduction is seen to have the largest effect close to Barcelona, with rather limited impacts on other European countries. Figs. 1(b)-(d) show how the climate-enhanced model versions differ from Fig. 1(a). The most important point is that the magnitude of these differences is very small relative to the absolute differences shown in Fig. 1(a). In fact,

Table 2: Reductions in TDEP-OXN due to 15% emission of NO_y and NH₃ in NL. Values give domain-mean changes in TDEP-OXN for the different base-cases. Units: mg(N) m⁻² yr⁻¹

Base-case	Base-value	Δ TDEP-OXN	
		NO _y	NH ₃
2010-Base	240.8	0.445	0.006
2050-Base	147.9	0.204	0.003
2050-A20	147.9	0.204	0.002
2050-bvoc	148.2	0.204	0.003
2050-KCO2	147.7	0.204	0.003

the differences are less than 0.5 mg(N) m⁻² yr⁻¹ for all climate scenarios. Similar results are seen for all countries.

Table 3: Reductions in TDEP-OXN due to 15% emission of NO_y and NH₃ in PL. Values give domain-mean changes in TDEP-OXN for the different base-cases. Units: mg(N) m⁻² yr⁻¹

Base-case	Base-value	Δ TDEP-OXN	
		NO _y	NH ₃
2010-Base	240.8	1.292	0.012
2050-Base	147.9	0.382	0.005
2050-A20	147.9	0.383	0.005
2050-bvoc	148.2	0.382	0.005
2050-KCO2	147.7	0.382	0.005

Table 4: Reductions in TDEP-OXN due to 15% emission of NO_y and NH₃ in ES. Values give domain-mean changes in TDEP-OXN for the different base-cases. Units: mg(N) m⁻² yr⁻¹

Base-case	Base-value	Δ TDEP-OXN	
		NO _y	NH ₃
2010-Base	240.8	1.920	0.010
2050-Base	147.9	0.704	0.002
2050-A20	147.9	0.705	0.002
2050-bvoc	148.2	0.706	0.002
2050-KCO2	147.7	0.704	0.002

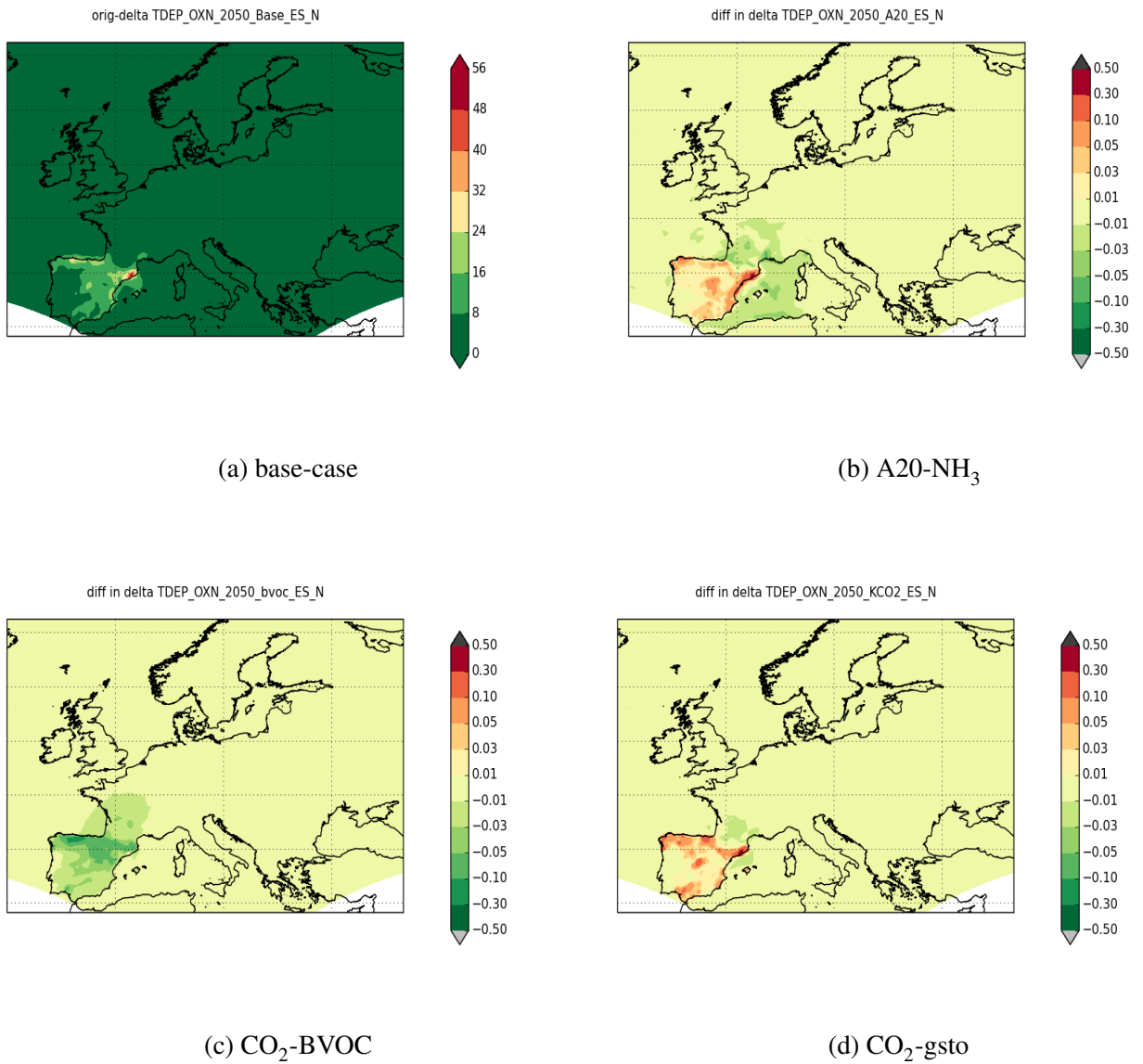


Figure 1:
 Source-receptor changes in 2050: the impact of NO_x emissions from ES on TDEP_OXN. Subfig (a) gives the base-case Δ TDEP_OXN for 2050. Remaining plots give the difference between Δ TDEP_OXN for different climate scenarios relative to that shown in (a). The scenarios are: (b) A20-NH₃, increased NH₃ (c) CO₂-inhibited isoprene emissions, and (d) CO₂-inhibited stomatal conductance. Note that colour-scale varies between (a) and the remaining plots.

Table 5: Reductions in TDEP-OXN due to 15% emission of NO_y and NH₃ in IT. Values give domain-mean changes in TDEP-OXN for the different base-cases. Units: mg(N) m⁻² yr⁻¹

Base-case	Base-value	Δ TDEP-OXN	
		NO _y	NH ₃
2010-Base	240.8	2.161	0.020
2050-Base	147.9	0.881	0.006
2050-A20	147.9	0.882	0.006
2050-bvoc	148.2	0.882	0.006
2050-KCO2	147.7	0.881	0.006

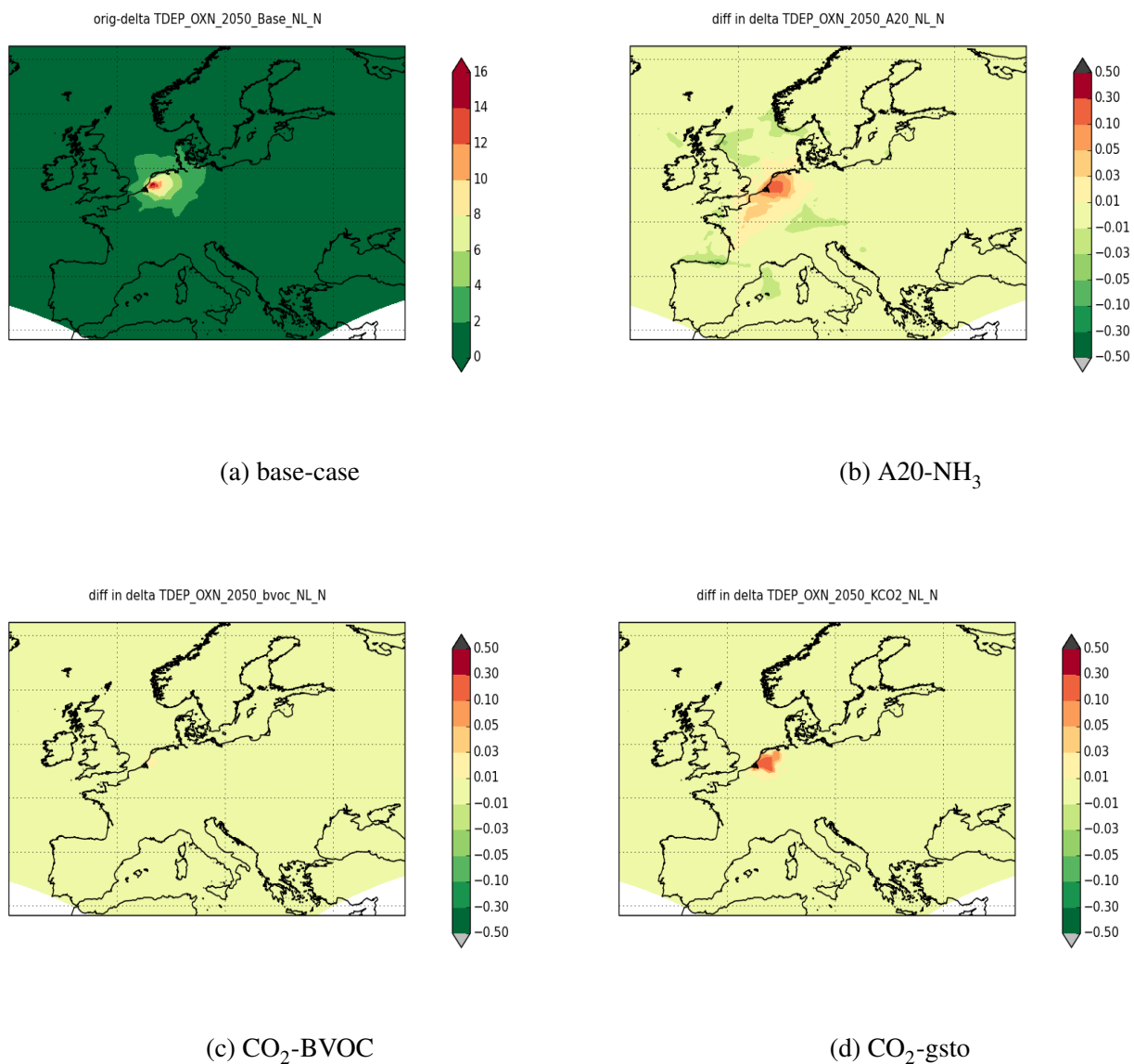


Figure 2:
 Source-receptor changes in 2050: the impact of NO_x emissions from NL on TDEP_OXN. Subfig (a) gives the base-case Δ TDEP_OXN for 2050. Remaining plots give the difference between Δ TDEP_OXN for different climate scenarios relative to that shown in (a). The scenarios are: (b) A20-NH₃, increased NH₃ (c) CO₂-inhibited isoprene emissions, and (d) CO₂-inhibited stomatal conductance. Note that colour-scale varies between (a) and the remaining plots.

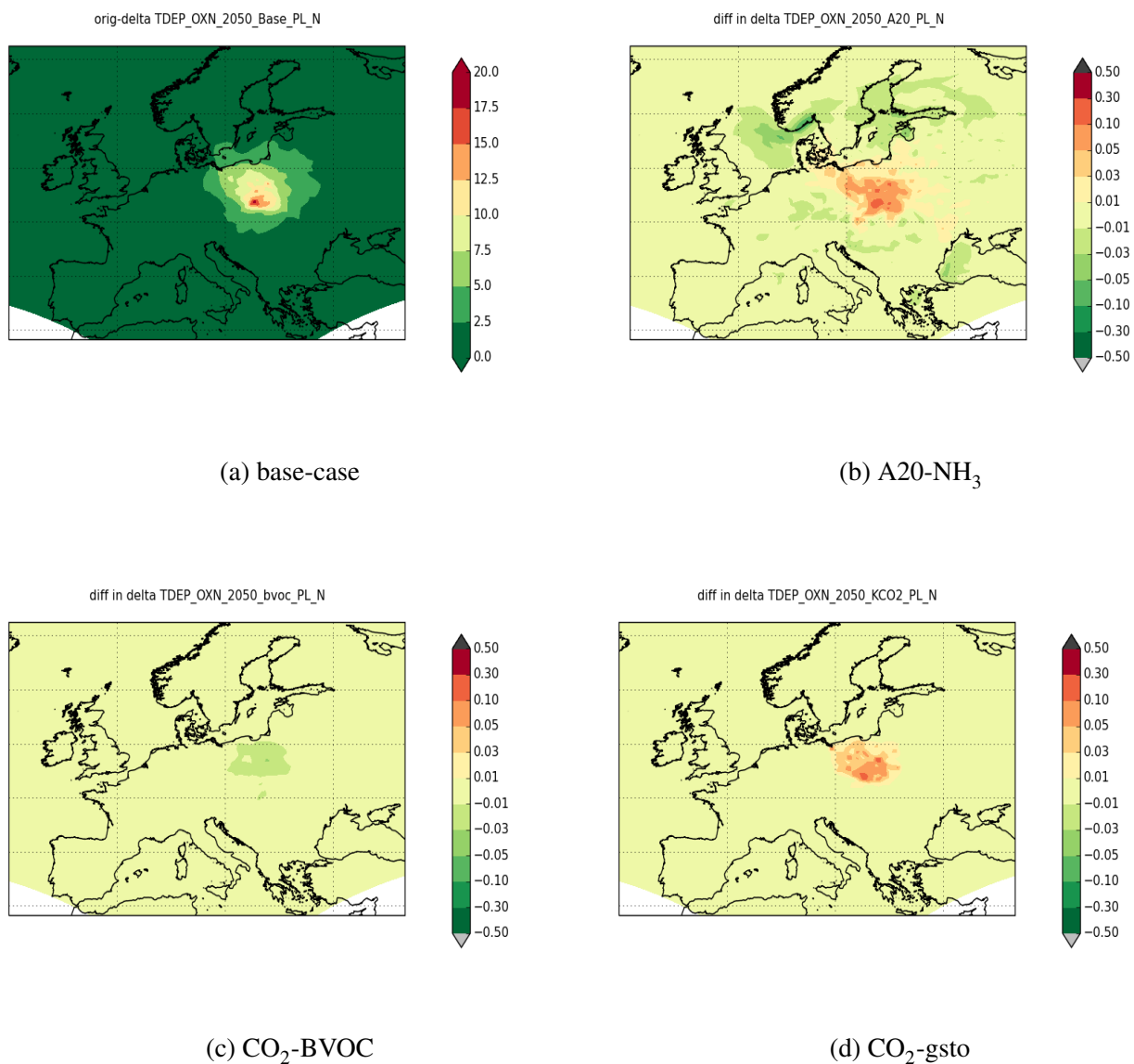


Figure 3:
 Source-receptor changes in 2050: the impact of NO_x emissions from PL on TDEP_OXN. Subfig (a) gives the base-case Δ TDEP_OXN for 2050. Remaining plots give the difference between Δ TDEP_OXN for different climate scenarios relative to that shown in (a). The scenarios are: (b) A20-NH₃, increased NH₃ (c) CO₂-inhibited isoprene emissions, and (d) CO₂-inhibited stomatal conductance. Note that colour-scale varies between (a) and the remaining plots.

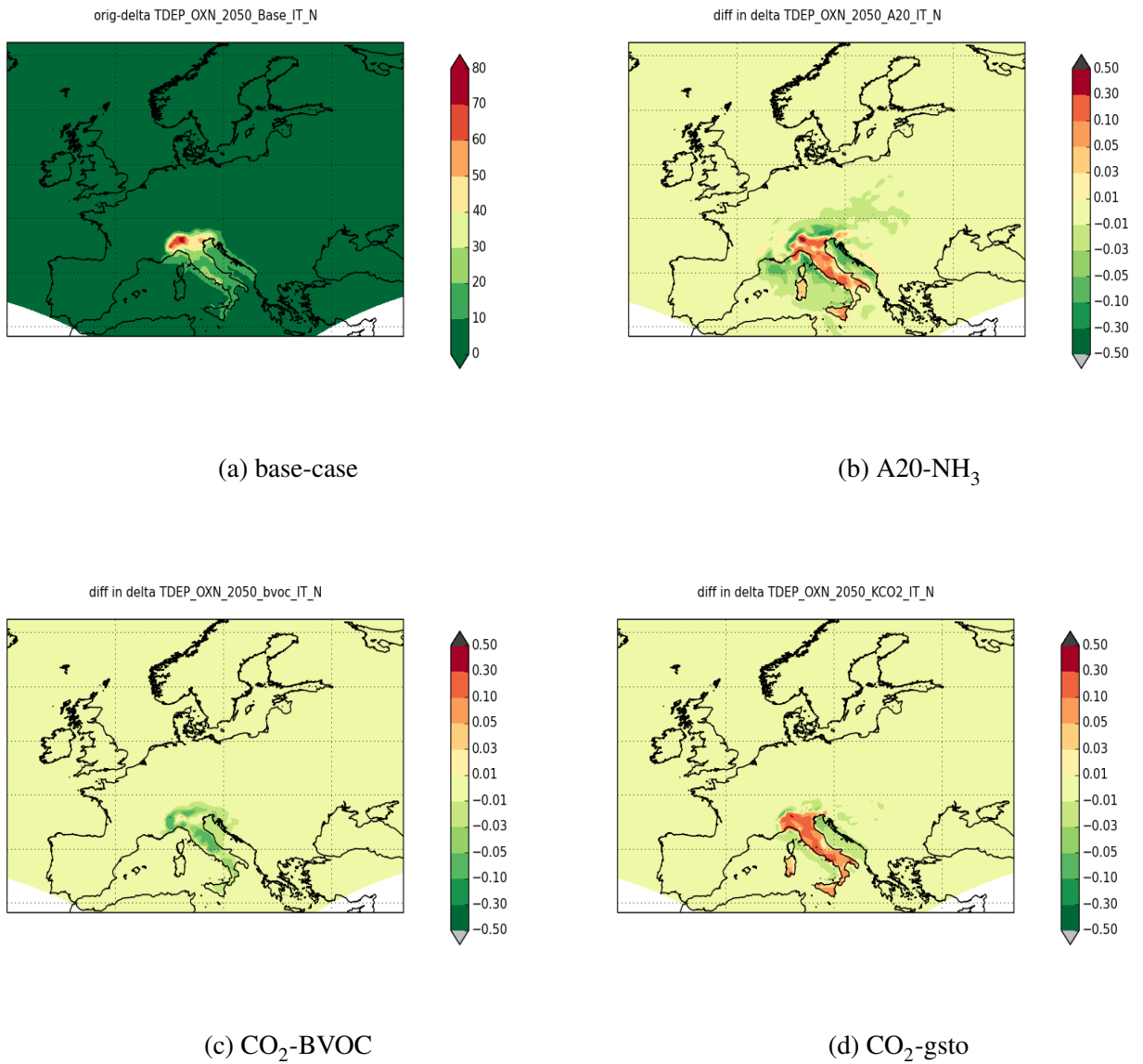


Figure 4:
 Source-receptor changes in 2050: the impact of NO_x emissions from IT on TDEP_OXN. Subfig (a) gives the base-case Δ TDEP_OXN for 2050. Remaining plots give the difference between Δ TDEP_OXN for different climate scenarios relative to that shown in (a). The scenarios are: (b) A20-NH₃, increased NH₃ (c) CO₂-inhibited isoprene emissions, and (d) CO₂-inhibited stomatal conductance. Note that colour-scale varies between (a) and the remaining plots.

Table 6: Reductions in TDEP-RDN due to 15% emission of NO_y and NH₃ in NL. Values give domain-mean changes in TDEP-RDN for the different base-cases. Units: mg(N) m⁻² yr⁻¹

Base-case	Base-value	Δ TDEP-RDN	
		NO _y	NH ₃
2010-Base	198.3	-0.004	0.611
2050-Base	221.3	-0.004	0.681
2050-A20	263.5	-0.005	0.818
2050-bvoc	221.3	-0.004	0.681
2050-KCO2	221.2	-0.004	0.681

3.2 NH_x deposition

Tables 6-9 present the results of the different SR calculations for total NH_x deposition, similar to those for NO_y deposition. These results are somewhat more complicated than those seen for NO_y deposition, in that (i) reduced NO_y emissions now lead to (very) small increases in TDEP-RDN, with now reduced NH₃ emissions leading as it should to decreases in TDEP-RDN, (ii) results for Δ TDEP are larger in 2050 than in 2010, and (iii) now one of the 2050 scenarios (A20) differs from the others. The 2050-A20 base-case involves higher NH₃ emissions from each country, which results in higher base-values of TDEP-RDN and a bigger effect of emission reduction. The 2050-Base, 2050-BVOC and 2050-KCO2 tests though produce almost identical results.

Figures 5-8 illustrate these SR calculations in more detail, this time for the impact of NH₃ emissions on reduced nitrogen deposition. As in Figs.1-4 above, Figs. 5(b)-(d) show how the climate-enhanced model versions differ from the 2050 base-case in Fig. 5(a). Unlike the case for TDEP-OXN, and as noted above, these TDEP-RDN results show that one climate-scenario, the A20 case, does produce S-R results which differ from the base-case.

For the other two climate scenarios (CO₂-BVOC and CO₂-*g_{sto}*) the differences are again very small relative to the absolute differences shown in Fig. 5(a). In fact, the differences are less than 0.5 mg(N) m⁻² yr⁻¹ for all climate scenarios. Similar results are seen for all countries.

Table 7: Reductions in TDEP-RDN due to 15% emission of NO_y and NH₃ in PL. Values give domain-mean changes in TDEP-RDN for the different base-cases. Units: mg(N) m⁻² yr⁻¹

Base-case	Base-value	Δ TDEP-RDN	
		NO _y	NH ₃
2010-Base	198.3	-0.009	1.575
2050-Base	221.3	-0.007	1.692
2050-A20	263.5	-0.008	2.036
2050-bvoc	221.3	-0.007	1.692
2050-KCO2	221.2	-0.007	1.691

Table 8: Reductions in TDEP-RDN due to 15% emission of NO_y and NH₃ in ES. Values give domain-mean changes in TDEP-RDN for the different base-cases. Units: mg(N) m⁻² yr⁻¹

Base-case	Base-value	Δ TDEP-RDN	
		NO _y	NH ₃
2010-Base	198.3	-0.009	1.629
2050-Base	221.3	-0.005	1.725
2050-A20	263.5	-0.007	2.074
2050-bvoc	221.3	-0.005	1.725
2050-KCO2	221.2	-0.005	1.724

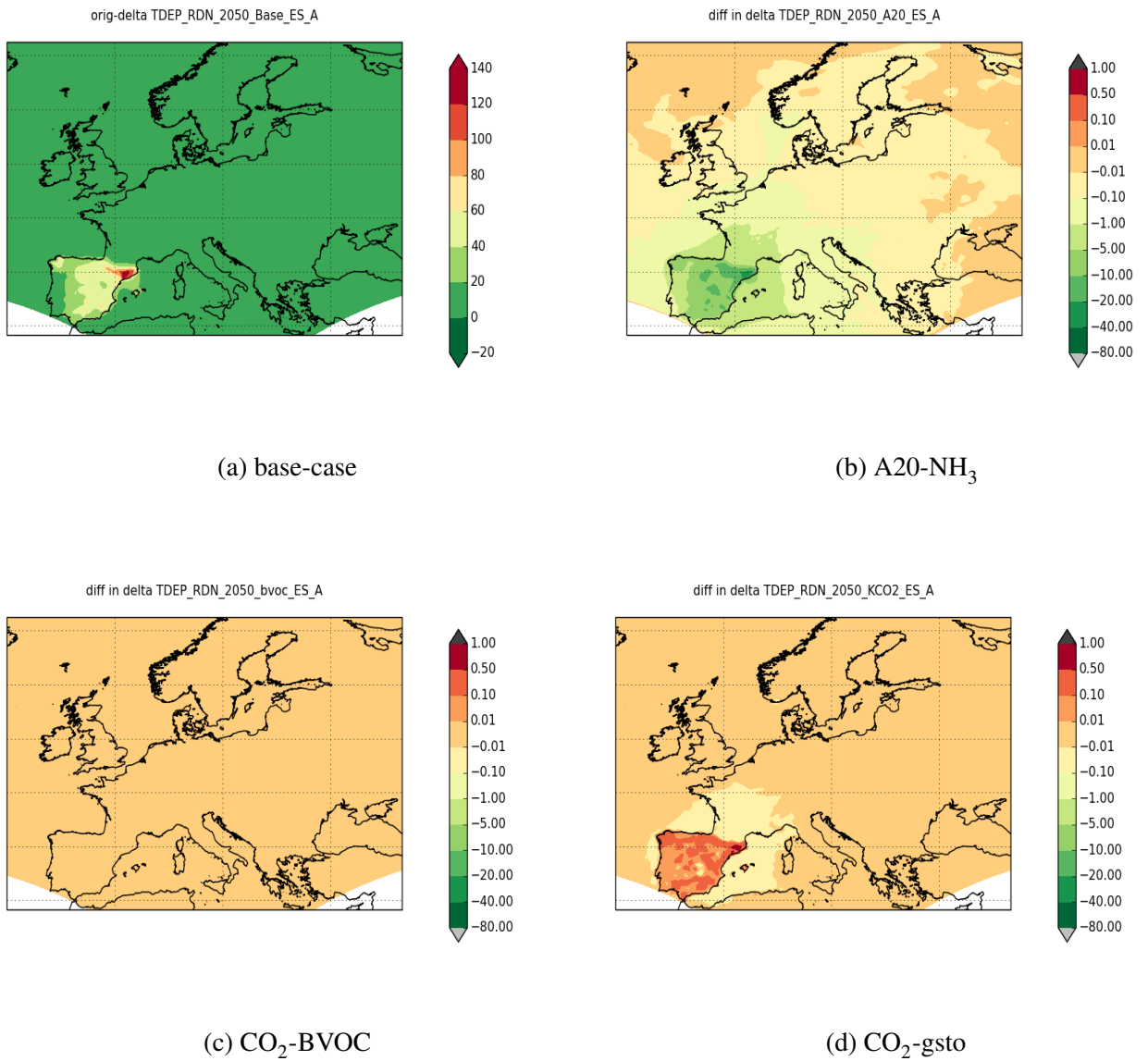


Figure 5:
 Source-receptor changes in 2050: the impact of NH₃ emissions from ES on TDEP_RDN. Subfig (a) gives the base-case Δ TDEP_RDN for 2050. Remaining plots give the difference between Δ TDEP_RDN for different climate scenarios relative to that shown in (a). The scenarios are: (b) A20-NH₃, increased NH₃ (c) CO₂-inhibited isoprene emissions, and (d) CO₂-inhibited stomatal conductance. Note that colour-scale varies between (a) and the remaining plots.

Table 9: Reductions in TDEP-RDN due to 15% emission of NO_y and NH₃ in IT. Values give domain-mean changes in TDEP-RDN for the different base-cases. Units: mg(N) m⁻² yr⁻¹

Base-case	Base-value	Δ TDEP-RDN	
		NO _y	NH ₃
2010-Base	198.3	-0.013	1.812
2050-Base	221.3	-0.009	1.996
2050-A20	263.5	-0.011	2.400
2050-bvoc	221.3	-0.009	1.996
2050-KCO2	221.2	-0.010	1.996

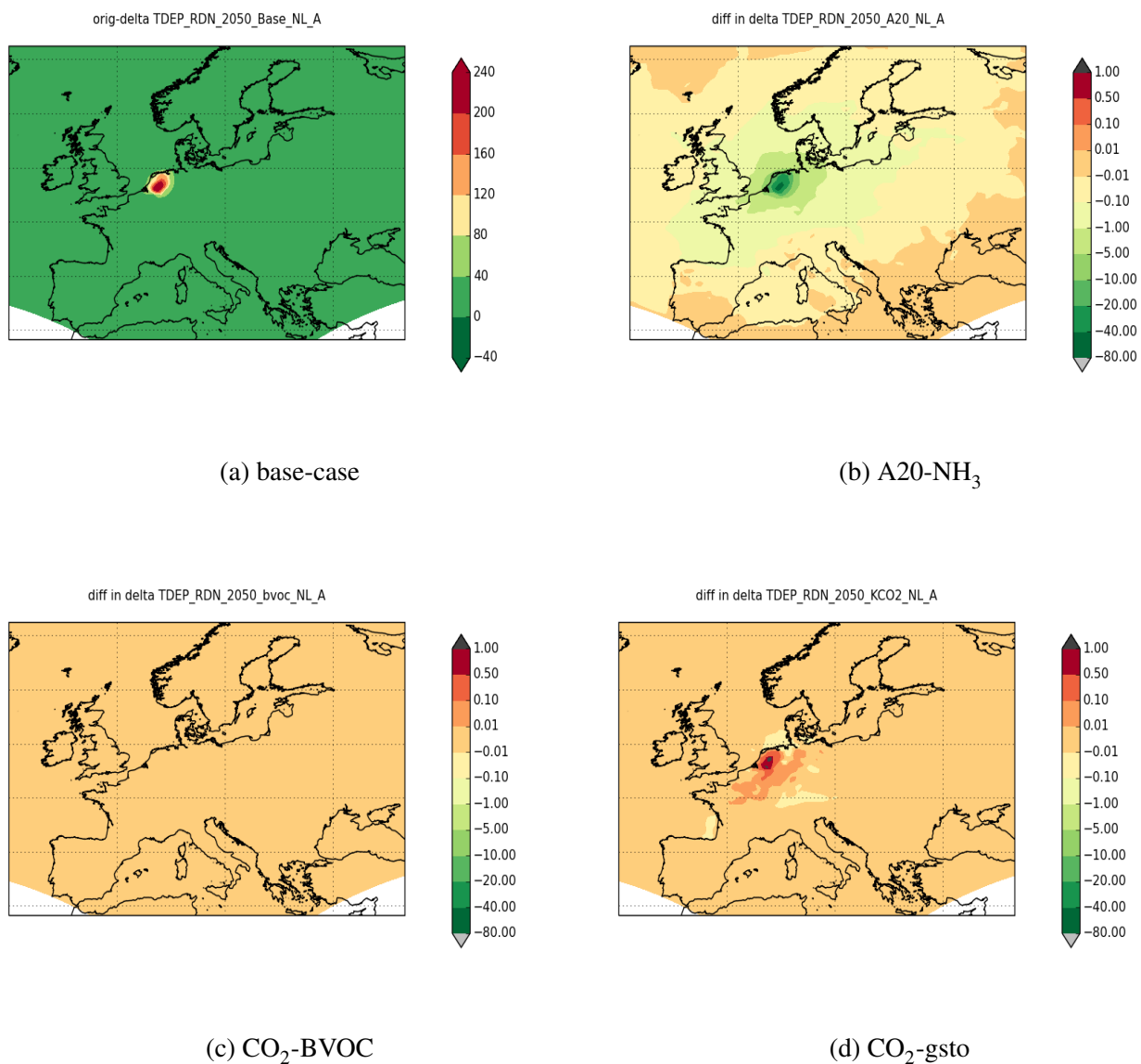


Figure 6:
 Source-receptor changes in 2050: the impact of NH₃ emissions from NL on TDEP_RDN. Subfig (a) gives the base-case Δ TDEP_RDN for 2050. Remaining plots give the difference between Δ TDEP_RDN for different climate scenarios relative to that shown in (a). The scenarios are: (b) A20-NH₃, increased NH₃ (c) CO₂-inhibited isoprene emissions, and (d) CO₂-inhibited stomatal conductance. Note that colour-scale varies between (a) and the remaining plots.

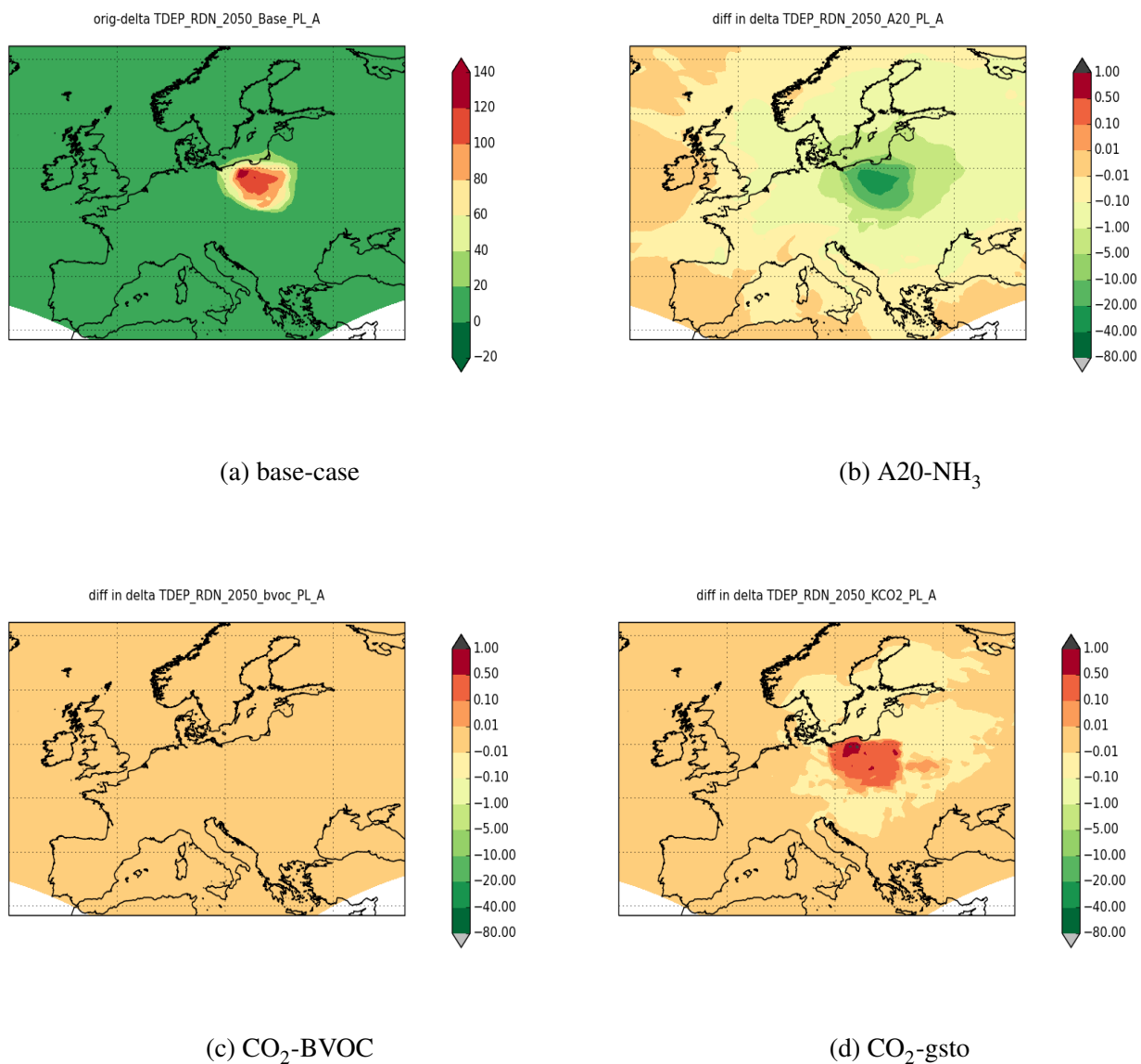


Figure 7:
 Source-receptor changes in 2050: the impact of NH₃ emissions from PL on TDEP_RDN. Subfig (a) gives the base-case Δ TDEP_RDN for 2050. Remaining plots give the difference between Δ TDEP_RDN for different climate scenarios relative to that shown in (a). The scenarios are: (b) A20-NH₃, increased NH₃ (c) CO₂-inhibited isoprene emissions, and (d) CO₂-inhibited stomatal conductance. Note that colour-scale varies between (a) and the remaining plots.

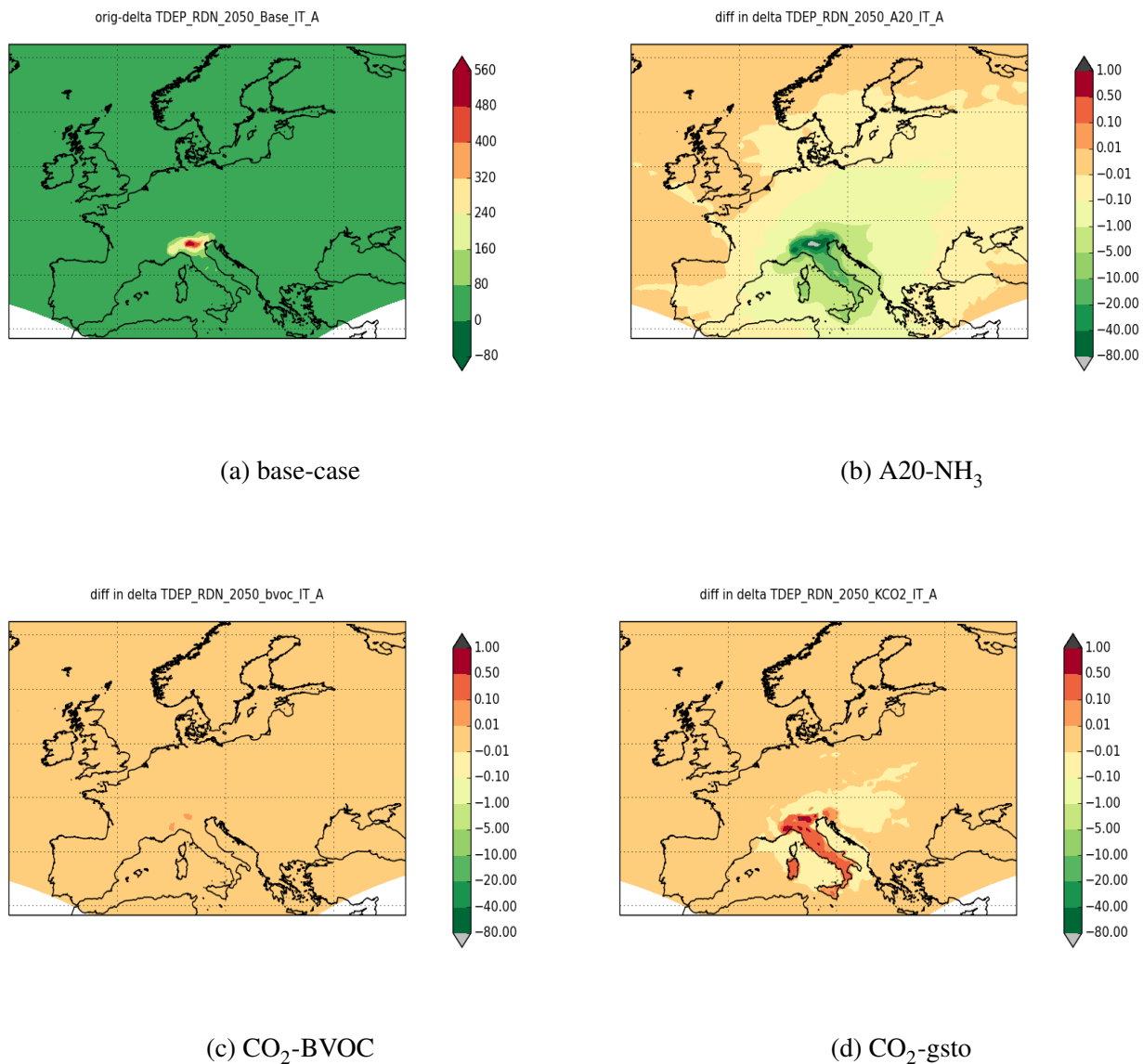


Figure 8:
 Source-receptor changes in 2050: the impact of NH₃ emissions from IT on TDEP_RDN. Subfig (a) gives the base-case Δ TDEP_RDN for 2050. Remaining plots give the difference between Δ TDEP_RDN for different climate scenarios relative to that shown in (a). The scenarios are: (b) A20-NH₃, increased NH₃ (c) CO₂-inhibited isoprene emissions, and (d) CO₂-inhibited stomatal conductance. Note that colour-scale varies between (a) and the remaining plots.

Table 10: Reductions in SOMO35 due to 15% emission of NO_y and NH₃ in NL. Values give domain-mean changes in SOMO35 for the different base-cases. Units: ppb.day

Base-case	Base-value	Δ SOMO35	
		NO _y	NH ₃
2010-Base	2985.4	-1.027	-0.384
2050-Base	2467.5	0.301	-0.185
2050-A20	2458.1	0.273	-0.162
2050-bvoc	2453.1	0.293	-0.185
2050-KCO2	2520.7	0.319	-0.188

3.3 Sum of Ozone over 35 ppb, SOMO35

Tables 10-13 present corresponding results the health-related ozone metric, SOMO35, and Figs. 9-12 illustrate the spatial variations and sensitivity to the climate scenario. It should be noted that the domain-mean values in the Tables are influenced by high SOMO35 over sea-areas (where O₃ deposition is low and hence concentrations high), but relative impacts should not be affected too much by this. The results for SOMO35 are more complex than seen for N-depositions above. For Netherlands for example, reduction of NO_y emissions from the 2010-Base case results in increases in SOMO35 even as a mean value over the full domain. Although the domain mean change for 2050 is now a reduction, Fig. 10 shows that a SOMO35 increase remains over the Netherlands itself (due to remaining NO_x titration) and decreases across the rest of Europe.

Indeed, in all of the 2050 base-cases, reduction of NO_y emissions results in decreases in mean SOMO35. Such behaviour is a result of the non-linearities inherent in ozone production, and such non-linearities are most apparent when NO_x emission densities are high - as they are in the Netherlands.

Another interesting feature of these SOMO35 results is that the differences between 2050 base-cases and Δ SOMO35 values are variable to some extent, e.g. Δ SOMO35 values for Dutch NO_y impacts change from 0.273 ppb.day for the 2050-A20 case to 0.318 for the 2050-KCO2 case. These differences reflect the fact that the different 2050 cases produce somewhat different base-fields for SOMO35, combined with some non-linearity in both ozone formation and the use of the 35 ppb threshold in the definition of SOMO35. On the other hand, although variable, the differences between 2050 Δ SOMO35 values are far smaller (especially for the Netherlands and Poland) than the difference between any 2050 and the 2010 base-case.

Table 11: Reductions in SOMO35 due to 15% emission of NO_y and NH₃ in PL. Values give domain-mean changes in SOMO35 for the different base-cases. Units: ppb.day

Base-case	Base-value	Δ SOMO35	
		NO _y	NH ₃
2010-Base	2985.4	0.472	-0.834
2050-Base	2467.5	1.579	-0.351
2050-A20	2458.1	1.550	-0.319
2050-bvoc	2453.1	1.553	-0.351
2050-KCO2	2520.7	1.687	-0.359

Table 12: Reductions in SOMO35 due to 15% emission of NO_y and NH₃ in ES. Values give domain-mean changes in SOMO35 for the different base-cases. Units: ppb.day

Base-case	Base-value	Δ SOMO35	
		NO _y	NH ₃
2010-Base	2985.4	7.413	-0.638
2050-Base	2467.5	7.961	-0.267
2050-A20	2458.1	7.920	-0.279
2050-bvoc	2453.1	7.855	-0.267
2050-KCO2	2520.7	8.059	-0.270

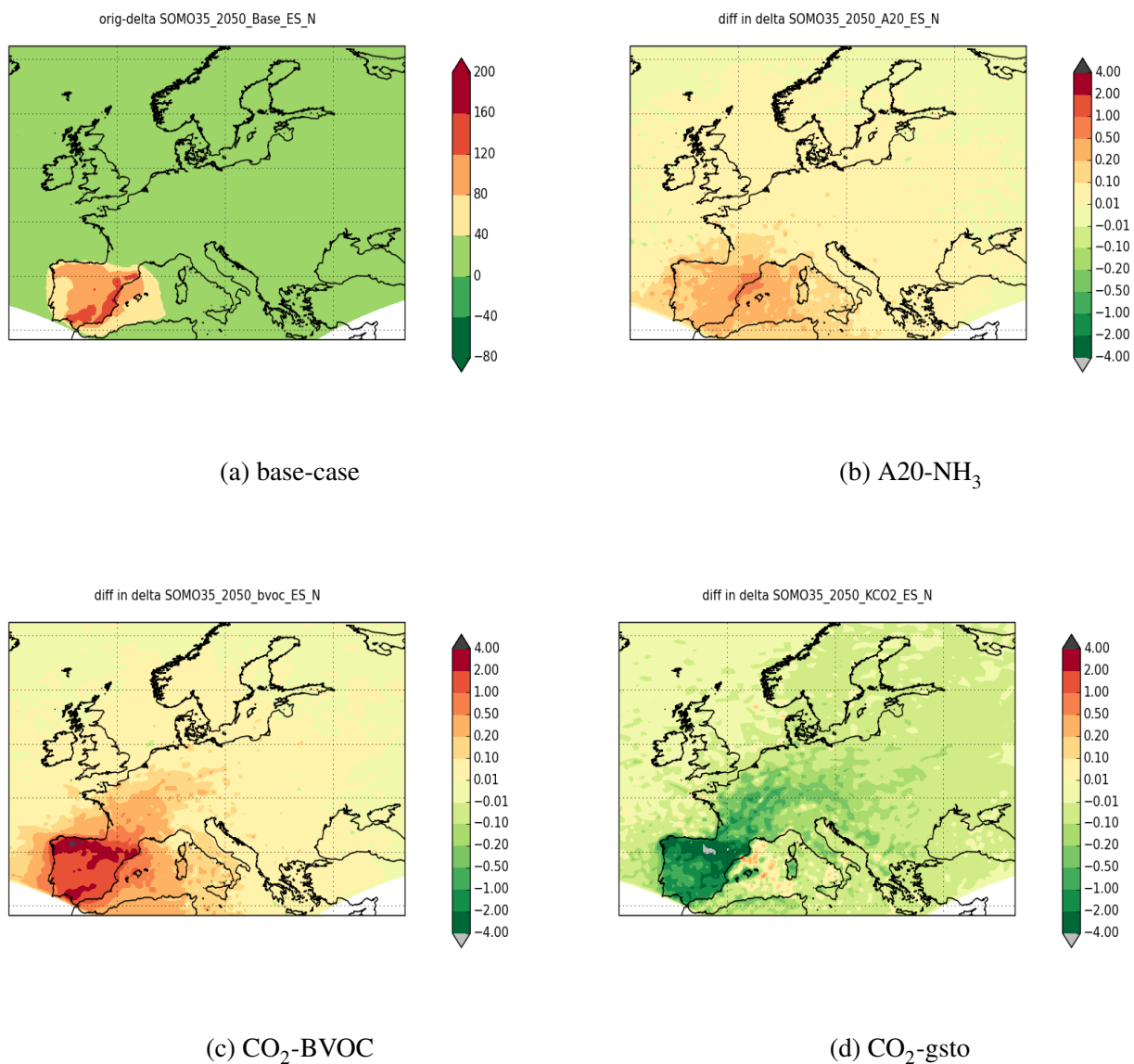


Figure 9:
 Source-receptor changes in 2050: the impact of NO_x emissions from ES on SOMO35. Subfig (a) gives the base-case Δ SOMO35 for 2050. Remaining plots give the difference between Δ SOMO35 for different climate scenarios relative to that shown in (a). The scenarios are: (b) A20-NH₃, increased NH₃ (c) CO₂-inhibited isoprene emissions, and (d) CO₂-inhibited stomatal conductance. Note that colour-scale varies between (a) and the remaining plots.

Table 13: Reductions in SOMO35 due to 15% emission of NO_y and NH₃ in IT. Values give domain-mean changes in SOMO35 for the different base-cases. Units: ppb.day

Base-case	Base-value	Δ SOMO35	
		NO _y	NH ₃
2010-Base	2985.4	7.575	-1.188
2050-Base	2467.5	8.817	-0.533
2050-A20	2458.1	8.748	-0.553
2050-bvoc	2453.1	8.756	-0.533
2050-KCO2	2520.7	8.900	-0.538

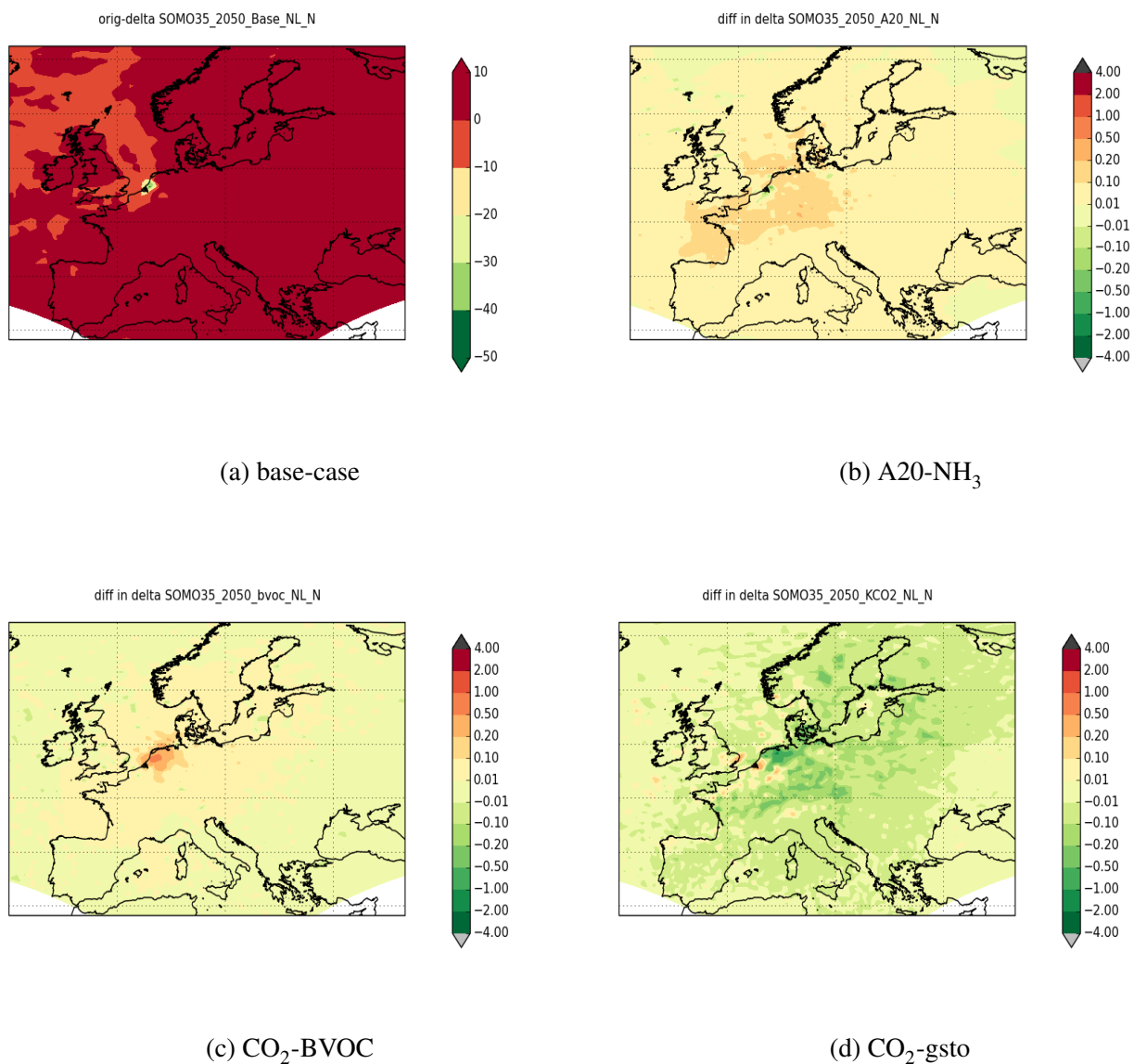


Figure 10:
 Source-receptor changes in 2050: the impact of NO_x emissions from NL on SOMO35. Subfig (a) gives the base-case Δ SOMO35 for 2050. Remaining plots give the difference between Δ SOMO35 for different climate scenarios relative to that shown in (a). The scenarios are: (b) A20-NH₃, increased NH₃ (c) CO₂-inhibited isoprene emissions, and (d) CO₂-inhibited stomatal conductance. Note that colour-scale varies between (a) and the remaining plots.

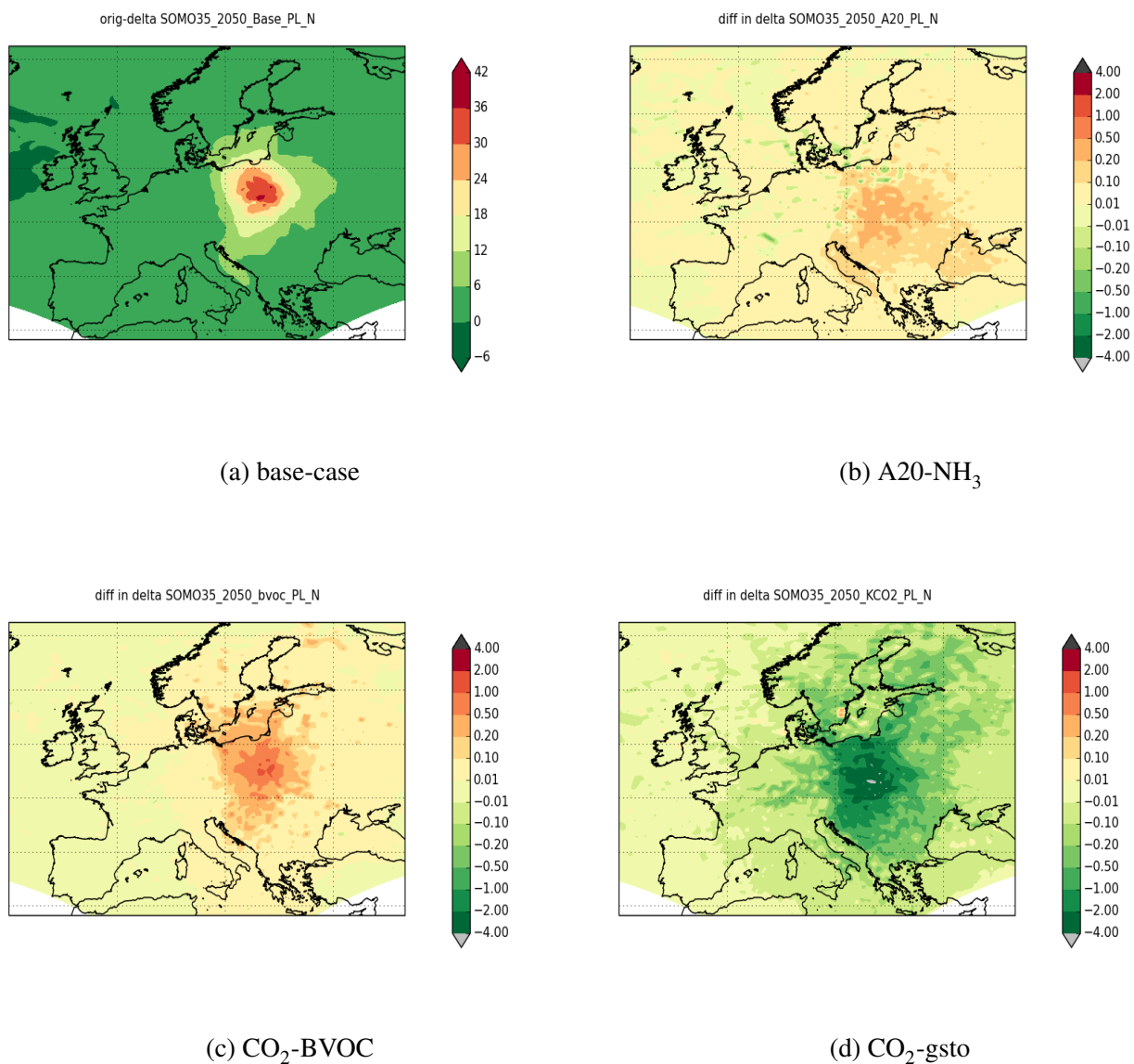


Figure 11:
 Source-receptor changes in 2050: the impact of NO_x emissions from PL on SOMO35. Subfig (a) gives the base-case Δ SOMO35 for 2050. Remaining plots give the difference between Δ SOMO35 for different climate scenarios relative to that shown in (a). The scenarios are: (b) A20-NH₃, increased NH₃ (c) CO₂-inhibited isoprene emissions, and (d) CO₂-inhibited stomatal conductance. Note that colour-scale varies between (a) and the remaining plots.

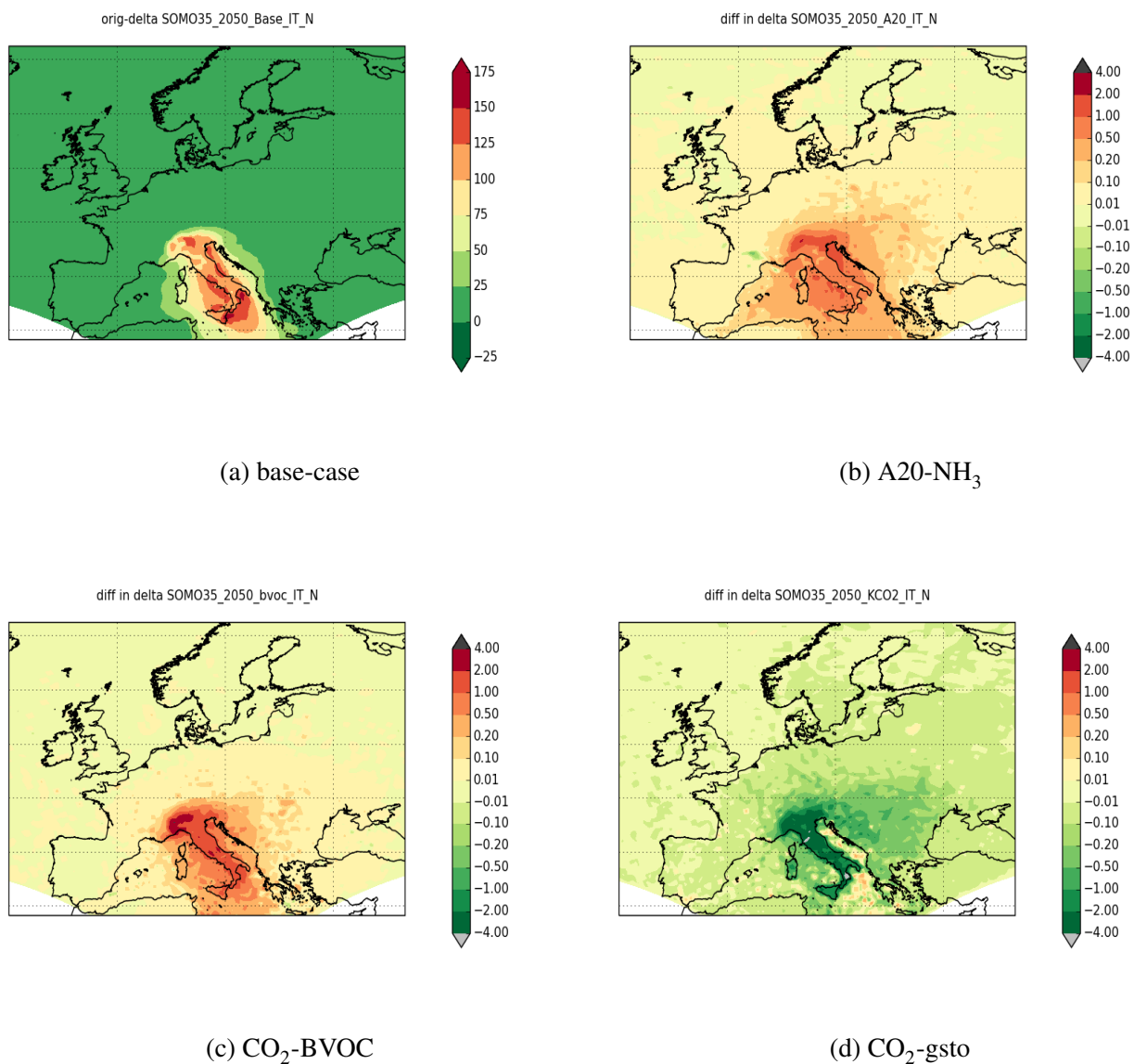


Figure 12:
 Source-receptor changes in 2050: the impact of NO_x emissions from IT on SOMO35. Subfig (a) gives the base-case Δ SOMO35 for 2050. Remaining plots give the difference between Δ SOMO35 for different climate scenarios relative to that shown in (a). The scenarios are: (b) A20-NH₃, increased NH₃ (c) CO₂-inhibited isoprene emissions, and (d) CO₂-inhibited stomatal conductance. Note that colour-scale varies between (a) and the remaining plots.

Table 14: Reductions in POD3-IAM-CR due to 15% emission of NO_y and NH₃ in NL. Values give domain-mean changes in POD3-IAM-CR for the different base-cases. Units: mmole O₃ m⁻² yr⁻¹

Base-case	Base-value	ΔPOD3	
		NO _y	NH ₃
2010-Base	6.1	-0.000	-0.001
2050-Base	5.2	0.001	-0.000
2050-A20	5.1	0.001	-0.000
2050-bvoc	5.1	0.001	-0.000
2050-KCO2	2.9	0.001	-0.000

3.4 Phyto-toxic ozone dose, POD

Tables 14-17 present corresponding results the vegetation risk indicator POD₃, as applied for a generic crop using methods recommended for integrated assessment mapping. Figs. 13-16 illustrate the spatial variations and sensitivity to the climate scenario.

POD is a measure of the ozone taken up by stomata, and with POD₃ only ozone fluxes of more than 3 nmole m⁻² s⁻¹ are counted towards the metric. In contrast to the metrics presented above, the values seen for ΔPOD3 are rather similar for most base-cases. The most dramatic difference is in the base-case values of POD₃ themselves, with the 2050-KCO2 scenario producing only about half of the base-value of the other scenarios. The 2050-KCO2 scenario also clearly stands out in Figs. 13-16.

Of course, 2050-KCO2 is a scenario that leads to a direct reduction in stomatal conductance and hence to ozone uptake. In addition, the use of the threshold of 3 nmole m⁻² s⁻¹ causes POD₃ to be much more sensitive to changes than total stomatal fluxes themselves (Tuovinen et al. 2007, 2009).

Table 15: Reductions in POD3-IAM-CR due to 15% emission of NO_y and NH₃ in PL. Values give domain-mean changes in POD3-IAM-CR for the different base-cases. Units: mmole O₃ m⁻² yr⁻¹

Base-case	Base-value	ΔPOD3	
		NO _y	NH ₃
2010-Base	6.1	0.006	-0.001
2050-Base	5.2	0.005	-0.000
2050-A20	5.1	0.005	-0.000
2050-bvoc	5.1	0.005	-0.000
2050-KCO2	2.9	0.003	-0.000

Table 16: Reductions in POD3-IAM-CR due to 15% emission of NO_y and NH₃ in ES. Values give domain-mean changes in POD3-IAM-CR for the different base-cases. Units: mmole O₃ m⁻² yr⁻¹

Base-case	Base-value	ΔPOD3	
		NO _y	NH ₃
2010-Base	6.1	0.010	-0.001
2050-Base	5.2	0.009	-0.000
2050-A20	5.1	0.008	-0.000
2050-bvoc	5.1	0.008	-0.000
2050-KCO2	2.9	0.006	-0.000

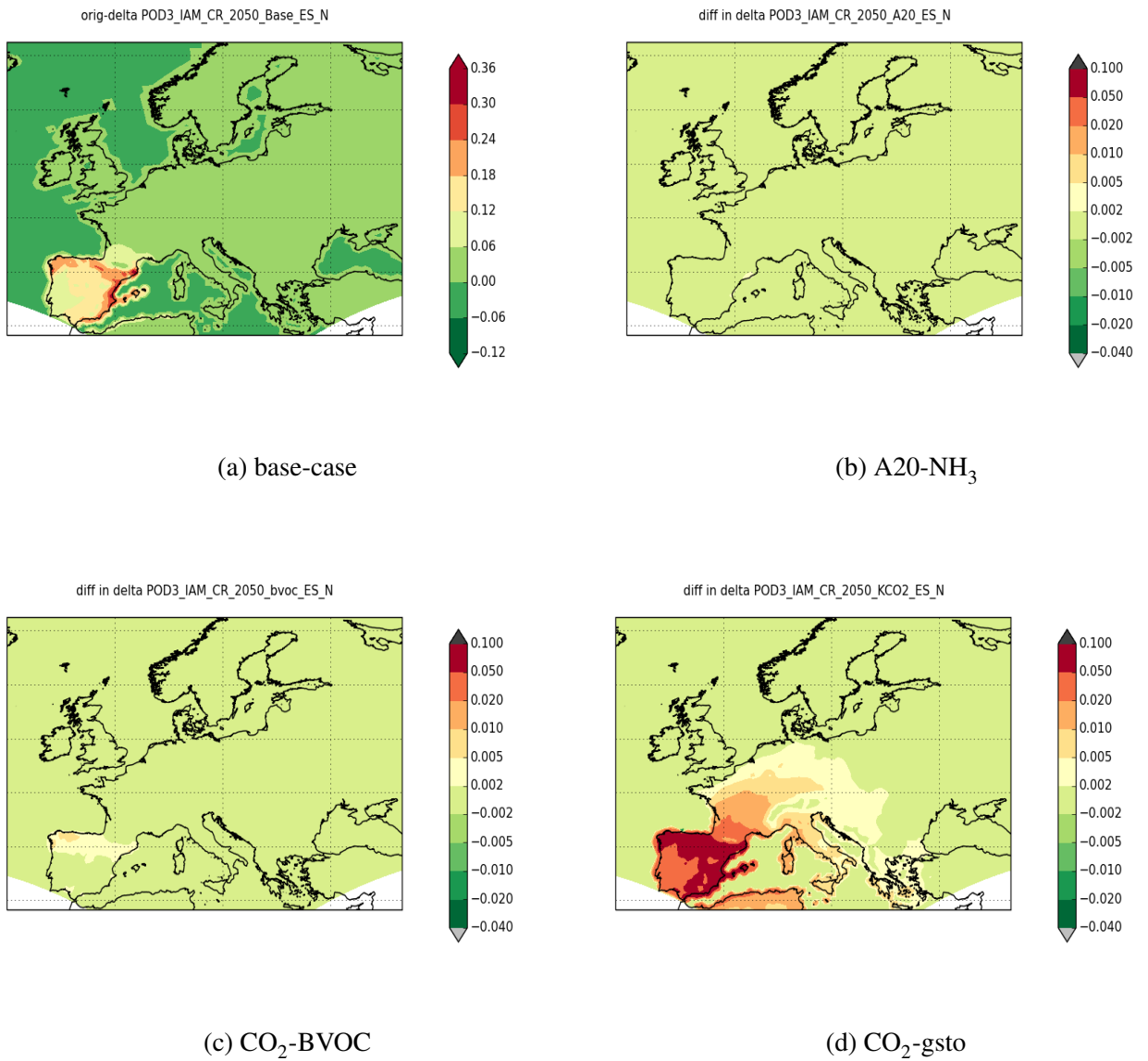


Figure 13:

Source-receptor changes in 2050: the impact of NO_x emissions from ES on POD3_IAM_CR. Subfig (a) gives the base-case Δ POD3_IAM_CR for 2050. Remaining plots give the difference between Δ POD3_IAM_CR for different climate scenarios relative to that shown in (a). The scenarios are: (b) A20-NH₃, increased NH₃ (c) CO₂-inhibited isoprene emissions, and (d) CO₂-inhibited stomatal conductance. Note that colour-scale varies between (a) and the remaining plots.

Table 17: Reductions in POD3-IAM-CR due to 15% emission of NO_y and NH₃ in IT. Values give domain-mean changes in POD3-IAM-CR for the different base-cases. Units: mmole O₃ m⁻² yr⁻¹

Base-case	Base-value	Δ POD3	
		NO _y	NH ₃
2010-Base	6.1	0.009	-0.001
2050-Base	5.2	0.010	-0.000
2050-A20	5.1	0.009	-0.000
2050-bvoc	5.1	0.009	-0.000
2050-KCO2	2.9	0.007	-0.000

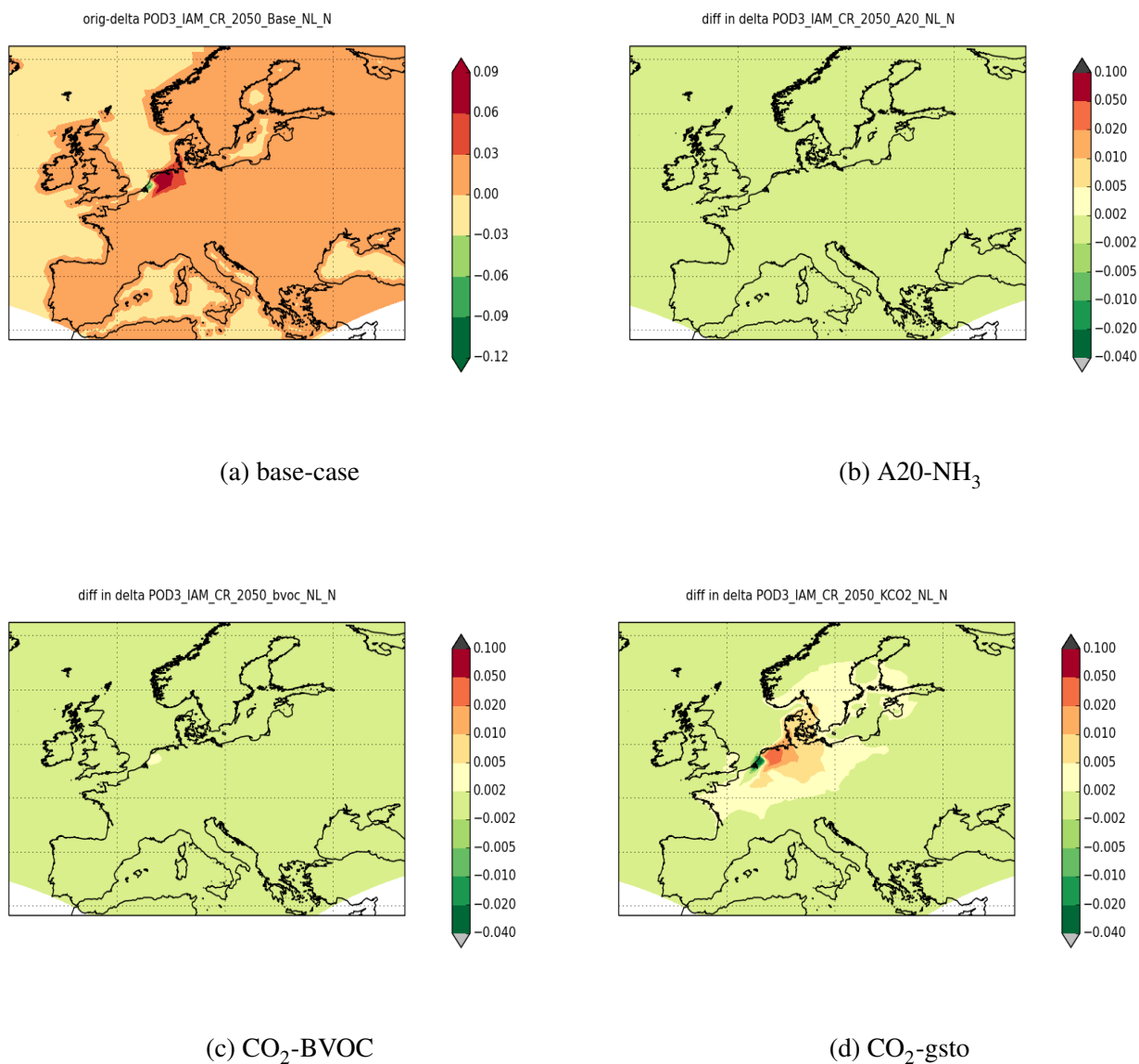


Figure 14:

Source-receptor changes in 2050: the impact of NO_x emissions from NL on POD3_IAM_CR. Subfig (a) gives the base-case Δ POD3_IAM_CR for 2050. Remaining plots give the difference between Δ POD3_IAM_CR for different climate scenarios relative to that shown in (a). The scenarios are: (b) A20-NH₃, increased NH₃ (c) CO₂-inhibited isoprene emissions, and (d) CO₂-inhibited stomatal conductance. Note that colour-scale varies between (a) and the remaining plots.

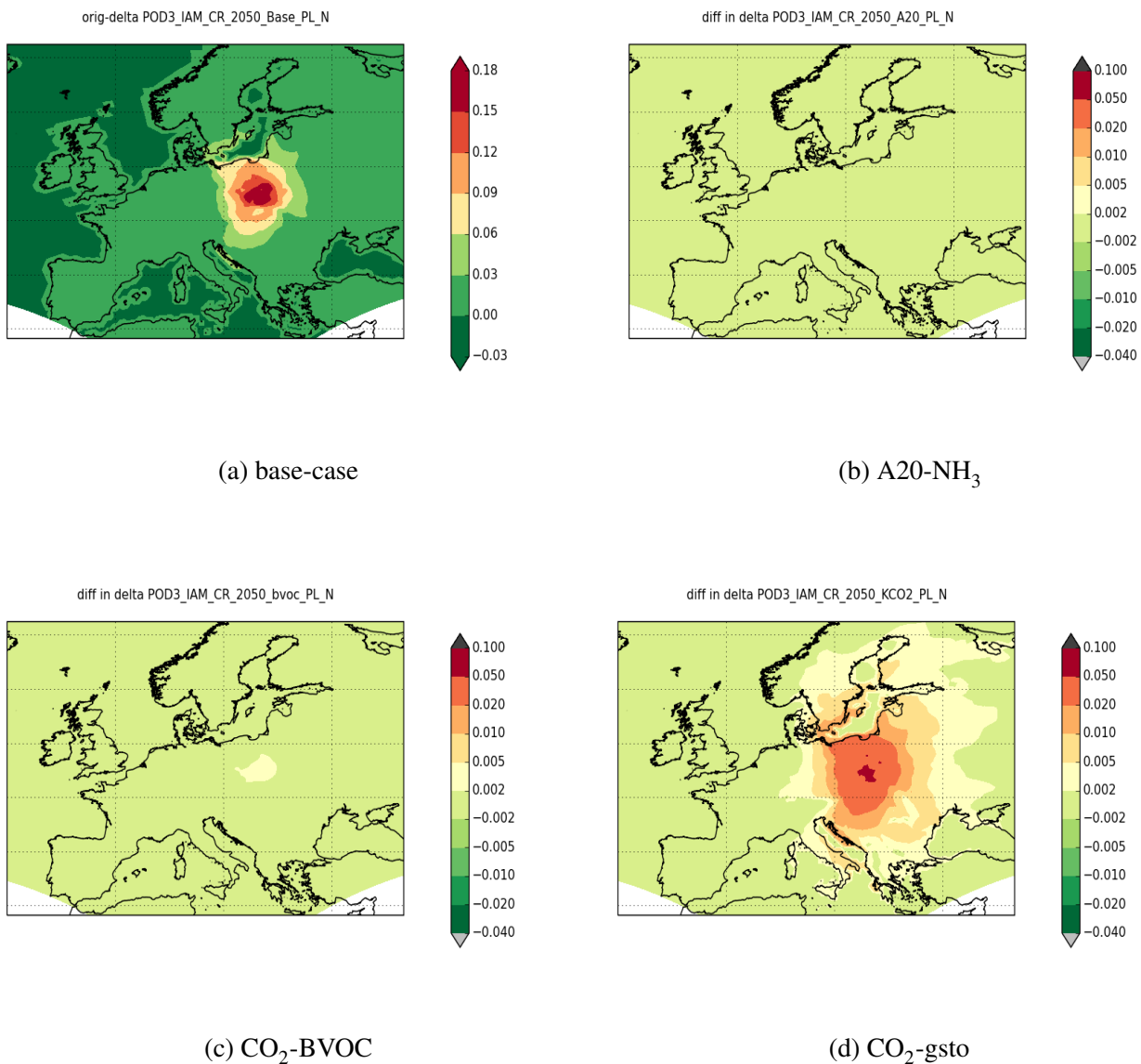


Figure 15:

Source-receptor changes in 2050: the impact of NO_x emissions from PL on POD3_IAM_CR. Subfig (a) gives the base-case Δ POD3_IAM_CR for 2050. Remaining plots give the difference between Δ POD3_IAM_CR for different climate scenarios relative to that shown in (a). The scenarios are: (b) A20-NH₃, increased NH₃ (c) CO₂-inhibited isoprene emissions, and (d) CO₂-inhibited stomatal conductance. Note that colour-scale varies between (a) and the remaining plots.

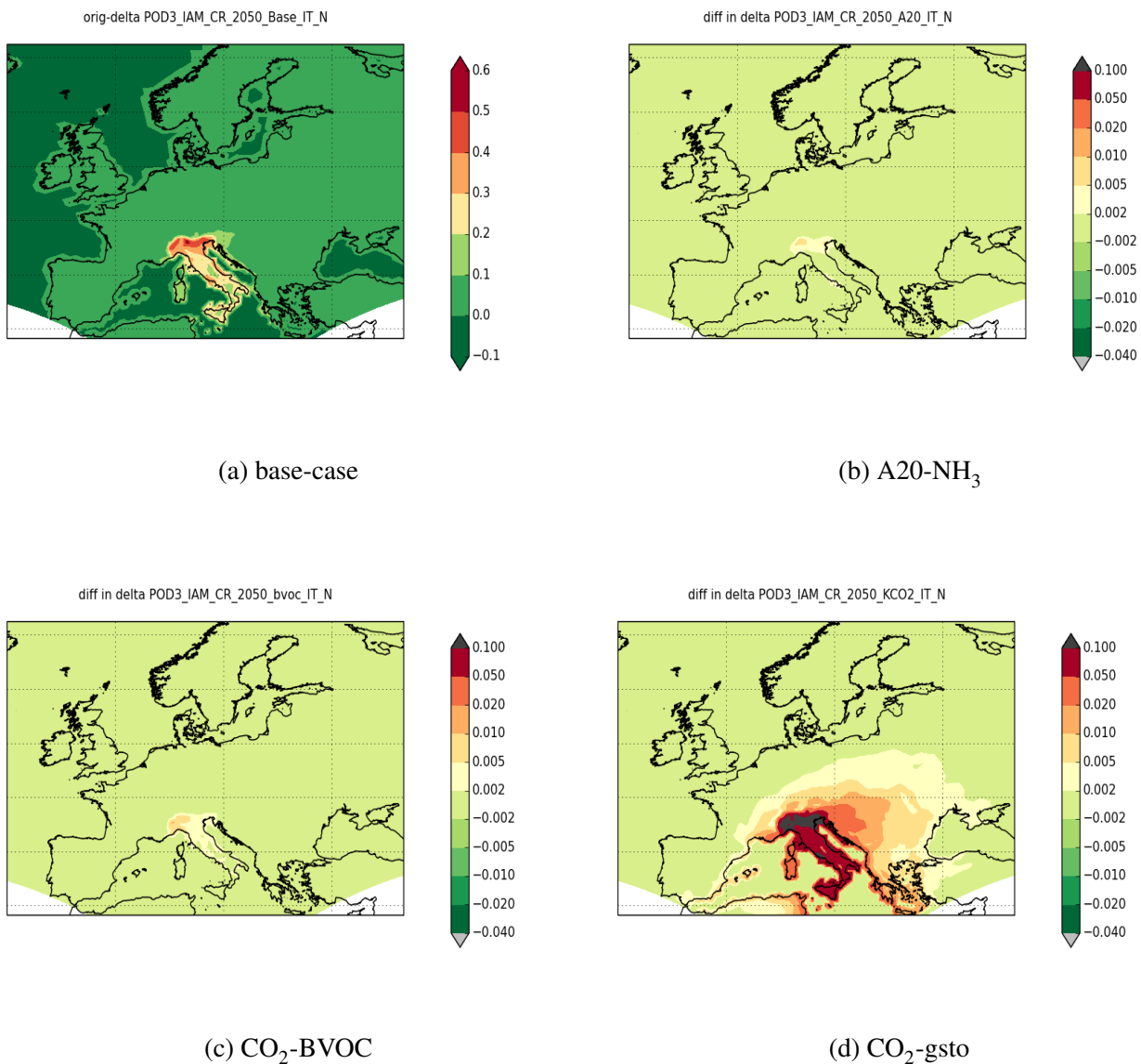


Figure 16:

Source-receptor changes in 2050: the impact of NO_x emissions from IT on POD3_IAM_CR . Subfig (a) gives the base-case $\Delta\text{POD3_IAM_CR}$ for 2050. Remaining plots give the difference between $\Delta\text{POD3_IAM_CR}$ for different climate scenarios relative to that shown in (a). The scenarios are: (b) A20-NH₃, increased NH₃ (c) CO₂-inhibited isoprene emissions, and (d) CO₂-inhibited stomatal conductance. Note that colour-scale varies between (a) and the remaining plots.

4 Milestones achieved

MS32 'Final' model-system ready. Commencement of source-receptor calculations.

Standard source-receptor calculations for the year 2013 can be found at www.emep.int. The source-receptor calculations for the future scenarios commenced towards the end of the ECLAIRE project.

5 Deviations and reasons

The commencement of source-receptor calculations was delayed compared to the original plan. Also during ECLAIRE it became apparent that in many cases the climate impacts are extremely uncertain, even with respect to the sign of the change in the case of the CO₂ inhibition of isoprene emissions (or of other BVOC emissions). There is thus no clear 'best' setup for 2050 scenarios, so a number of possible futures needs to be explored. The main need as seen by e.g. IIASA for the GAINS model is to get an improved understanding of how S-R relationships based upon current understanding and climate will change depending on different climate assumptions, so the work was re-focused on this aspect.

6 Publications

Bergström, R., Hallquist, M., Simpson, D., Wildt, J. & Mentel, T. F. Biotic stress: a significant contributor to organic aerosol in Europe? *Atmospheric Chemistry and Physics*, 2014, 14, 13643-13660

Colette, A., Granier, C., Hodnebrog, ., Jakobs, H., Maurizi, A., Nyiri, A., Rao, S., Amann, M., Bessagnet, B., D'Angiola, A., Gauss, M., Heyes, C., Klimont, Z., Meleux, F., Memmesheimer, M., Mieville, A., Roul, L., Russo, F., Schucht, S., Simpson, D., Stordal, F., Tampieri, F. & Vrac, M. Future air quality in Europe: a multi-model assessment of projected exposure to ozone *Atmos. Chem. Physics*, 2012, 12, 10613-10630

Engardt, M., Simpson, D. and Granat, L., Historical and projected (1900 to 2050) deposition of sulphur and nitrogen in Europe, 2015, in preparation for ECLAIRE special issue.

Fowler, D., Steadman, C. E., Stevenson, D., Coyle, M., Rees, R. M., Skiba, U. M., Sutton, M. A., Cape, J. N., Dore, A. J., Vieno, M., Simpson, D., Zaehle, S., Stocker, B. D., Rinaldi, M., Facchini, M. C., Flechard, C. R., Nemitz, E., Twigg, M., Erisman, J. W. & Galloway, J. N. Effects of global change during the 21st century on the nitrogen cycle *Atmospheric Chemistry and Physics Discussions*, 2015, 15, 1747-1868

Langner, J., Engardt, M., Baklanov, A., Christensen, J. H., Gauss, M., Geels, C., Hedegaard, G. B., Nuterman, R., Simpson, D., Soares, J., Sofiev, M., Wind, P. & Zakey, A. A multi-model study of impacts of climate change on surface ozone in Europe *Atmos. Chem. Physics*, 2012, 12, 10423-10440

Langner, J., Engardt, M. & Andersson, C. European summer surface ozone 1990–2100 *Atmos. Chem. Physics*, 2012, 12, 10097-10105

Simpson, D., Christensen, J., Engardt, M., Geels, C., Nyiri, A., Soares, J., Sofiev, M., Wind, P. & Langner, J. Impacts of climate and emission changes on nitrogen deposition in Europe: a multi-model study *Atmos. Chem. Physics*, 2014, 14, 6995-7017

Simpson, D., Arneth, A., Mills, G., Solberg, S. & Uddling, J. Ozone - the persistent menace, interactions with the N cycle and climate change, *Current Op. Environ. Sust.*, 2014, 9-10, 9-19

Sutton, M. A., Reis, S., Riddick, S. N., Dragosits, U., Nemitz, E., Theobald, M. R., Tang, Y. S., Braban, C. F., Vieno, M., Dore, A. J., Mitchell, R. F., Wanless, S., Daunt, F., Fowler, D., Blackall, T. D., Milford, C., Flechard, C. R., Loubet, B., Massad, R., Cellier, P., Personne, E., Coheur, P. F., Clarisse, L., Van Damme, M., Ngadi, Y., Clerbaux, C., Skjærff, C. A., Geels, C., Hertel, O., Wichink Kruit, R. J., Pinder, R. W., Bash, J. O., Walker, J. T., Simpson, D., Horváth, L., Misselbrook, T. H., Bleeker, A., Dentener, F. & de Vries, W. Towards a climate-dependent paradigm of ammonia emission and deposition *Phil. Trans. R. Soc. B: Biol. Sci.*, 2013, 368, 20130166

Tuovinen, J.-P., Hakola, H., Karlsson, P. E. & Simpson, D. Air Pollution Risks to Northern European Forests in a Changing Climate 5 *Climate Change, Air Pollution and Global Challenges Understanding and Perspectives from Forest Research*, Elsevier, Oxford, UK, 2013, 13, 77 - 99 (Eds: D. Matyssek, R., Clarke, N., Cudlin, P., Mikkelsen, T., Tuovinen, J.-P., Wieser, G. & Paoletti, E.)

7 Meetings

Participation in ECLAIRE annual meetings, plus several WP7 meetings to organise and analyse the model results.

8 List of Documents/Annexes:

n.a.

References

Amann, M., Derwent, D., Fosberg, B., Hänninen, O., Hurley, F., de Leeuw, F., Krzyzanowski, M., Liu, S. J., Mandin, C., Schneider, J., Schwarze, P., and Simp-

- son, D.: Health risks of ozone from long-range transboundary air pollution, World Health Organisation, European Centre for Environment and Health Bonn Office, joint WHO/Convention Task Force on the Health Aspects of Air Pollution, 2008.
- Arneth, A., Niinemets, U., Pressley, S., Bäck, J., Hari, P., Karl, T., Noe, S., Prentice, I. C., Serca, D., Hickler, T., Wolf, A., and Smith, B.: Process-based estimates of terrestrial ecosystem isoprene emissions: incorporating the effects of a direct CO₂-isoprene interaction, *Atmos. Chem. Physics*, 7, 31–53, URL <http://www.atmos-chem-phys.net/7/31/2007/>, 2007.
- Bergström, R., Hallquist, M., Simpson, D., Wildt, J., and Mentel, T. F.: Biotic stress: a significant contributor to organic aerosol in Europe?, *Atmospheric Chemistry and Physics*, 14, 13 643–13 660, doi:10.5194/acp-14-13643-2014, URL <http://www.atmos-chem-phys.net/14/13643/2014/>, 2014.
- Fagerli, H. and Aas, W.: Trends of nitrogen in air and precipitation: Model results and observations at EMEP sites in Europe, 1980–2003, *Environ. Poll.*, 154, 448–461, 2008.
- Klingberg, J., Engardt, M., Uddling, J., Karlsson, P. E., and Pleijel, H.: Ozone risk for vegetation in the future climate of Europe based on stomatal ozone uptake calculations, *Tellus Series A - Dyn. Met. Ocean.*, 63, 174–187, doi:10.1111/j.1600-0870.2010.00465.x, 2011.
- Langner, J., Engardt, M., and Andersson, C.: European summer surface ozone 1990–2100, *Atmos. Chem. Physics*, 12, 10 097–10 105, doi:10.5194/acp-12-10097-2012, URL <http://www.atmos-chem-phys.net/12/10097/2012/>, 2012a.
- Langner, J., Engardt, M., Baklanov, A., Christensen, J. H., Gauss, M., Geels, C., Hede-gaard, G. B., Nuterman, R., Simpson, D., Soares, J., Sofiev, M., Wind, P., and Zakey, A.: A multi-model study of impacts of climate change on surface ozone in Europe, *Atmos. Chem. Physics*, 12, 10 423–10 440, doi:10.5194/acp-12-10423-2012, URL <http://www.atmos-chem-phys.net/12/10423/2012/>, 2012b.
- LRTAP: Mapping critical levels for vegetation, in: *Manual on Methodologies and Criteria for Mapping Critical Loads and Levels and Air Pollution Effects, Risks and Trends. Revision of 2009*, edited by Mills, G., UNECE Convention on Long-range Transboundary Air Pollution. International Cooperative Programme on Effects of Air Pollution on Natural Vegetation and Crops, updated version available at www.icpmapping.com/, 2009.
- Mills, G., Pleijel, H., Braun, S., Büker, P., Bermejo, V., Calvo, E., Danielsson, H., Emberson, L., Grünhage, L., Fernández, I. G., Harmens, H., Hayes, F., Karlsson,

- P.-E., and Simpson, D.: New stomatal flux-based critical levels for ozone effects on vegetation, *Atmos. Environ.*, 45, 5064 – 5068, doi:10.1016/j.atmosenv.2011.06.009, 2011.
- Possell, M. and Hewitt, C. N.: Isoprene emissions from plants are mediated by atmospheric CO₂ concentrations, *Global Change Biol.*, 17, 1595–1610, doi: 10.1111/j.1365-2486.2010.02306.x, URL <http://dx.doi.org/10.1111/j.1365-2486.2010.02306.x>, 2011.
- Possell, M., Hewitt, C., and Beerling, D.: The effects of glacial atmospheric CO₂ concentrations and climate on isoprene emissions by vascular plants, *Global Change Biol.*, 11, 60–69, doi:10.1111/j.1365-2486.2004.00889.x, 2005.
- Sakalli, A. and Simpson, D.: Towards the use of dynamic growing seasons in a chemical transport model, *Biogeosciences*, 9, 5161–5179, doi:10.5194/bg-9-5161-2012, URL <http://www.biogeosciences.net/9/5161/2012/>, 2012.
- Simpson, D., Butterbach-Bahl, K., Fagerli, H., Kesik, M., Skiba, U., and Tang, S.: Deposition and Emissions of Reactive Nitrogen over European Forests: A Modelling Study, *Atmos. Environ.*, 40, 5712–5726, doi:10.1016/j.atmosenv.2006.04.063, 2006.
- Simpson, D., Benedictow, A., Berge, H., Bergström, R., Emberson, L. D., Fagerli, H., Flechard, C. R., Hayman, G. D., Gauss, M., Jonson, J. E., Jenkin, M. E., Nyíri, A., Richter, C., Semeena, V. S., Tsyro, S., Tuovinen, J.-P., Valdebenito, A., and Wind, P.: The EMEP MSC-W chemical transport model – technical description, *Atmos. Chem. Physics*, 12, 7825–7865, doi:10.5194/acp-12-7825-2012, URL <http://www.atmos-chem-phys.net/12/7825/2012/acp-12-7825-2012.html>, 2012.
- Simpson, D., Arneth, A., Mills, G., Solberg, S., and Uddling, J.: Ozone - the persistent menace; interactions with the N cycle and climate change, *Current Op. Environ. Sust.*, 9-10, 9–19, doi:<http://dx.doi.org/10.1016/j.cosust.2014.07.008>, sI: System dynamics and sustainability, 2014a.
- Simpson, D., Christensen, J., Engardt, M., Geels, C., Nyiri, A., Soares, J., Sofiev, M., Wind, P., and Langner, J.: Impacts of climate and emission changes on nitrogen deposition in Europe: a multi-model study, *Atmos. Chem. Physics*, 14, 6995–7017, doi: 10.5194/acp-14-0073-2014, URL <http://www.atmos-chem-phys.net/14/0073/2014/acp-14-0073-2014.html>, 2014b.
- Skjøth, C. A. and Geels, C.: The effect of climate and climate change on ammonia emissions in Europe, *Atmos. Chem. Physics*, 13, 117–128, doi:10.5194/acp-13-117-2013, URL <http://www.atmos-chem-phys.net/13/117/2013/>, 2013.

- Sutton, M. A., Reis, S., Riddick, S. N., Dragosits, U., Nemitz, E., Theobald, M. R., Tang, Y. S., Braban, C. F., Vieno, M., Dore, A. J., Mitchell, R. F., Wanless, S., Daunt, F., Fowler, D., Blackall, T. D., Milford, C., Flechard, C. R., Loubet, B., Massad, R., Cellier, P., Personne, E., Coheur, P. F., Clarisse, L., Van Damme, M., Ngadi, Y., Clerbaux, C., Skjøth, C. A., Geels, C., Hertel, O., Wichink Kruit, R. J., Pinder, R. W., Bash, J. O., Walker, J. T., Simpson, D., Horváth, L., Misselbrook, T. H., Bleeker, A., Dentener, F., and de Vries, W.: Towards a climate-dependent paradigm of ammonia emission and deposition, *Phil. Trans. R. Soc. B: Biol. Sci.*, 368, 20130166, doi: 10.1098/rstb.2013.0166, URL <http://rstb.royalsocietypublishing.org/content/368/1621/20130166.abstract>, 2013.
- Tuovinen, J.-P., Simpson, D., Ashmore, M., Emberson, L., and Gerosa, G.: Robustness of modelled ozone exposures and doses, *Environ. Poll.*, 146, 578–586, 2007.
- Tuovinen, J.-P., Emberson, L., and Simpson, D.: Modelling ozone fluxes to forests for risk assessment: status and prospects, *Annals of Forest Science*, 66, 401, URL dx.doi.org/10.1051/forest/2009024, 2009.
- Wilkinson, M. J., Monson, R. K., Trahan, N., Lee, S., Brown, E., Jackson, R. B., Polley, H. W., Fay, P. A., and Fall, R.: Leaf isoprene emission rate as a function of atmospheric CO₂ concentration, *Global Change Biol.*, 15, 1189–1200, doi: 10.1111/j.1365-2486.2008.01803.x, 2009.